PAPER

High-performance and flexible photodetectors based on chemical vapor deposition grown two-dimensional In_2Se_3 nanosheets

IOP Publishing Nanotechnology
Nanotechnology 29 (2018) 445205 (6pp) https://doi.org/10.1088/1361-6528/aadc73

High-performance and flexible photodetectors based on chemical vapor deposition grown two-dimensional In_2Se_3 nanosheets

Wei Feng[1,5], Feng Gao[2], Yunxia Hu[2], Mingjin Dai[2], Hang Li[3], Lifeng Wang[4] and PingAn Hu[2,5]

[1] Department of Chemistry and Chemical Engineering, College of Science, Northeast Forestry University, Harbin, 150040, People's Republic of China
[2] Key Lab of Microsystem and Microstructure of Ministry of Education, Harbin Institute of Technology, Harbin, 150080, People's Republic of China
[3] Changchun Institute of Optics, Fine Mechanics and Physics, Chinese Academy of Sciences, Changchun, 130033, People's Republic of China
[4] Institute for Frontier Materials, Deakin University, 75 Pigdons Road, Waurn Ponds, Geelong, Victoria 3216, Australia

E-mail: wfeng@nefu.edu.cn and hupa@hit.edu.cn

Received 8 June 2018, revised 14 August 2018
Accepted for publication 23 August 2018
Published 5 September 2018

Abstract

Two-dimensional (2D) In_2Se_3 with unique optical and electrical properties has great potential in next generation optoelectronics and multilevel phase-change memories. Here, for the first time, we report high-performance rigid and flexible photodetectors based on chemical vapor deposition (CVD) grown 2D In_2Se_3. Both rigid and flexible 2D In_2Se_3 photodetectors show a broadband response range from ultraviolet (254 nm) to visible light (700 nm). High photoresponsivities of 578 and 363 $A \cdot W^{-1}$ are achieved using rigid and flexible 2D In_2Se_3 photodetectors, respectively, under 700 nm light illumination, which are higher than those of photodetectors based on mechanically exfoliated 2D In_2Se_3 and physical vapor deposition grown 2D In_2Se_3. Furthermore, flexible 2D In_2Se_3 photodetectors show good mechanical durability and photoresponse stability under repeated bending tests. A high and stable photoresponse provides an opportunity for CVD-grown 2D In_2Se_3 applications in flexible optoelectronic and photovoltaic devices.

Supplementary material for this article is available online

Keywords: In_2Se_3, photodetector, flexible devices, two-dimensional materials

(Some figures may appear in colour only in the online journal)

1. Introduction

Graphene opens the door to research two-dimensional (2D) materials with exciting properties and novel applications in contrast to their bulk counterparts [1–4]. Compared to other low-dimensional materials (one-dimensional and zero-dimensional materials), 2D compounds are more compatible with traditional semiconductor microfabrication techniques and are easily integrated into complex structures to meet the requirements of novel electronic and optoelectronic devices [5–7]. Layered materials exhibit strong intralayer bonding together with a weak interlayer van der Waals interaction, which offers the possibility of readily fabricating atomically thin monolayers or few-layer nanosheets from their parent bulk materials via chemical or micromechanical

[5] Authors to whom any correspondence should be addressed.

exfoliation methods. Until now, vast 2D layered materials have been investigated, including graphene [1, 8], h-BN (hexagonal boron nitride) [9, 10], transition-metal dichalcogenides (TMDs: MoS_2 [3, 11], WSe_2 [12, 13], etc) and III–VI group compounds (GaSe [14, 15], InSe [16, 17] and In_2Se_3 [18, 19], etc). Compared to gapless graphene and insulating h-BN, semiconducting TMDs have been extensively explored for applications in next generation field-effect transistors (FETs), photodetectors and logic circuits.

In_2Se_3, a typical III–VI binary layered chalcogenide, with a narrow direct bandgap of 1.3 eV, is a candidate material for applications in optoelectronics [18, 20], phase-change memory devices [21, 22] and ionic batteries [23]. In contrast to TMDs, research on 2D In_2Se_3 is limited [18, 19, 24, 25]. The crystalline–crystalline ($\alpha \rightarrow \beta$) phase transformation associated with changes in the electrical transport properties of 2D In_2Se_3 crystals has been demonstrated [26], which paves the way for multilevel phase-change memories in a single material system. Photodetectors based on mechanically exfoliated 2D In_2Se_3 and physical vapor deposition (PVD)-grown 2D In_2Se_3 nanosheets exhibit a good photoresponse and broadband photoresponse range from ultraviolet to near-infrared [18, 25], and their photocurrents strongly depend on gate bias [27]. Compared to 2D TMDs, 2D In_2Se_3 shows a more tunable thickness-dependent optical bandgap from 1.45 eV (25 nm) to 2.8 eV (3.1 nm) [28], making it promising for applications in near-infrared, visible and near-UV photodetection. Therefore, 2D In_2Se_3 is a very attractive material and needs to be further investigated. Though high-performance photodetectors based on mechanically exfoliated 2D In_2Se_3 and PVD-grown 2D In_2Se_3 have been previously demonstrated [18, 25], mechanical exfoliation is difficult for large-scale fabrication and it is easier to introduce more defects under high temperature conditions using the PVD method [25]. Large-scale 2D In_2Se_3 has been successfully synthesized using the CVD method, which is conducted under mild conditions, including low temperature and atmospheric conditions [29]. However, the optoelectronic properties of CVD-grown 2D In_2Se_3 nanosheets have never been investigated in detail. Moreover, early reports mainly focus on rigid 2D In_2Se_3 photodetectors; the research on flexible 2D In_2Se_3 photodetectors is limited. Therefore, it is important and necessary to explore optoelectronic properties of CVD-grown 2D In_2Se_3.

Here, for the first time, we report on high-performance rigid and flexible photodetectors based on CVD-grown 2D In_2Se_3. Photodetectors based on CVD-grown 2D In_2Se_3 nanosheets on both rigid SiO_2/Si substrates and flexible polyethylene terephthalate (PET) substrates were fabricated. Both the rigid and flexible CVD-grown 2D In_2Se_3 nanosheet photodetectors showed high photoresponse with a wide photoresponse range from ultraviolet (254 nm) to visible light (700 nm). High photoresponsivities of 578 and 363 $A \cdot W^{-1}$ were obtained from the rigid and flexible photodetectors, respectively, under 700 nm light illumination, which are higher than those of mechanically exfoliated and PVD-grown 2D In_2Se_3. The flexible 2D In_2Se_3 photodetectors showed excellent mechanical durability and photoresponse stability after 10 repeated cycles of the bending test.

2. Method

2.1. CVD synthesis of atomically thin In_2Se_3 nanosheets

The 2D In_2Se_3 was synthesized by a 2-inch tube furnace-based CVD system. Se powders (99.998%, Aladdin, 200 mg) were placed at an upstream heating zone and were heated for 23 mins to 350 °C. In_2O_3 powders (99.99%, Aladdin, 30 mg) were placed at a downstream heating zone and were heated for 44 min to 660 °C. The reaction was kept at 660 °C for 20 min. The vapor was carried from the upstream zone to the downstream zone by carrier gases (H_2:Ar = 7:13 sccm), and 2D In_2Se_3 nanosheets were deposited on mica substrates ($1 \times 1\ cm^2$) placed 2 cm away from the downstream heating zone (i.e. from the In_2O_3 power). After the reaction, the system was cooled down to room temperature.

2.2. Characterizations of as-grown 2D In_2Se_3

Optical images of the In_2Se_3 nanoflakes were taken with an OLYMPUS BX41. The microstructure of the 2D In_2Se_3 nanosheets were determined by transmission electron microscopy (TEM, Tacnai-G2 F30, accelerating voltage of 300 kV), selective area electron diffraction (SAED) and HR-TEM. The thickness of the 2D In_2Se_3 was determined by atomic force microscopy (AFM, Nanoscope IIIa Vecco).

2.3. Fabrication and characterization of 2D In_2Se_3 FETs and photodetectors

As-grown 2D In_2Se_3 nanosheets were transferred onto 300 nm SiO_2/Si and flexible PET substrates with the PMMA-assisted method, and 5/50 nm Cr/Au metal electrodes were fabricated by thermal evaporation with copper shadow masks. The electronic and optoelectronic properties of the 2D In_2Se_3 were measured using a Keithley 4200 SCS with a Lakeshore probe station under ambient environment. Mono-chromatic lights of 254, 365, 490, 610 and 700 nm were obtained using a 500 W xenon lamp with different optical filters, and the bandwidth of the used filters was 10 nm. The intensities of the illumination light source were determined by a power and energy meter (Model 372, Scienteck).

3. Result and discussion

In_2Se_3 is a typical III–VI group layered semiconductor. Bulk In_2Se_3 is composed of vertically stacked Se–In–Se–In–Se sheets and each sheet is weakly bound to its neighboring sheet by van der Waals force (figure 1(a)). 2D In_2Se_3 nanosheets were synthesized on mica substrates via catalyst-free van der Waals epitaxy CVD process (more details in section 2). The as-grown 2D In_2Se_3 nanosheets were first identified by optical contrast. A typical optical image of as-synthesized 2D In_2Se_3 nanosheets is shown in figure 1(b). The whole mica substrate

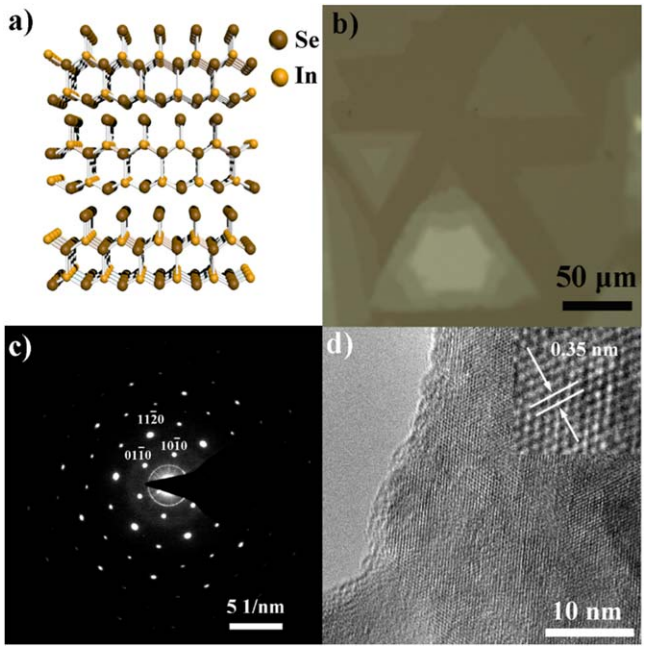

Figure 1. Characterizations of 2D In_2Se_3: (a) crystal structure of In_2Se_3. (b) Optical image of as-grown In_2Se_3 nanosheets on mica substrate. (c) A SAED pattern of as-grown In_2Se_3 nanosheet. (d) HR-TEM image of as-grown In_2Se_3 nanosheet. The inset is reverse Fourier transform pattern.

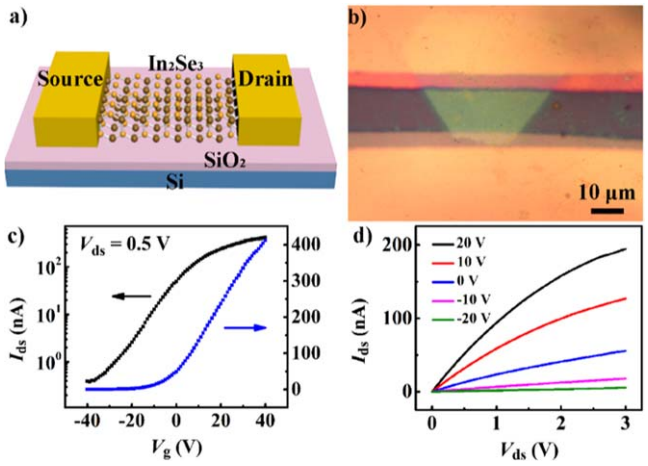

Figure 2. Electronic properties of 2D In_2Se_3 FETs. (a) Schematic diagram of back-gated 2D In_2Se_3 FETs configuration. (b) Optical image of 2D In_2Se_3 FETs. (c) The transfer curves of 2D In_2Se_3 FETs measured at $V_{ds} = 0.5$ V. (d) The corresponding output curves of 2D In_2Se_3 FETs.

$(1 \times 1\,cm^2)$ was covered by randomly dispersed 2D In_2Se_3 nanosheets. The lateral size was up to 100 μm and different optical contrasts of 2D In_2Se_3 nanosheets represented different thicknesses (see more discussions in our earlier study [29]). The thickness of the as-grown 2D In_2Se_3 nanosheets was estimated by optical contrast and further determined by AFM. Figure S1, which is available online at stacks.iop.org/NANO/29/445205/mmedia, is a typical AFM image of a 2D In_2Se_3 nanosheet. The thickness of the thinnest nanosheet was ~1 nm, corresponding to the monolayer sample. The microstructure of the as-grown 2D In_2Se_3 nanosheets was characterized by TEM. Figure 1(c) is a typical SAED pattern of the as-synthesized 2D In_2Se_3 nanosheet. It was a 6-fold symmetry structure, demonstrating the as-synthesized 2D In_2Se_3 nanosheets orientated along the ⟨001⟩ zone axis with good crystalline quality. Figure 1(d) is the HR-TEM image of the as-synthesized 2D In_2Se_3 nanosheets and shows an ideal hexagonal lattice structure with a distance of 0.35 nm, corresponding to the α-In_2Se_3 lattice constant in the (100) direction [18].

To explore the electronic properties of the 2D In_2Se_3 nanosheets, 2D In_2Se_3 nanosheets were transferred to SiO_2/Si substrates and back-gated FETs were fabricated (see section 2 for more detail). Figure 2(a) is the 3D model of the 2D In_2Se_3 FETs with a back-gated configuration. 2D In_2Se_3 nanosheets, a 300 nm SiO_2 layer, Cr/Au and the p-doping silicon worked as the channel materials, dielectric materials, source/drain and gate electrode, respectively. Figure 2(b) is a typical optical image of 2D In_2Se_3 FETs with a channel length of 10 μm and a channel width of 20 μm. The thickness of the 2D In_2Se_3 channel was determined to be 6 nm by AFM, as shown in figure S2. In this study, all measurements were conducted in an ambient environment. Figures 2(c) and (d) are the room temperature gate-dependent transfer and output curves, respectively. The 2D In_2Se_3 FETs show a typical n-type semiconducting transport behavior since the current decreased with an applied gate voltage sweeping from positive values to negative values in the transfer curves. This n-type conductance behavior was consistent with bulk In_2Se_3 and totally different from the p-type semiconducting behavior of the PVD-grown 2D In_2Se_3 via a higher temperature process [25], because a higher temperature decomposes In_2Se_3 powders and results in selenium-rich environments. To evaluate the electronic transport properties of the 2D In_2Se_3, the field-effect electron mobility (μ) was calculated by the equation $\mu = [L/(W \times (\varepsilon_0\varepsilon_r/d) \times V_{ds})] \times dI_{ds}/dV_g$, where $L = 10\,\mu$m is the channel length, $W = 20\,\mu$m is the channel width (as shown in figure 2(b)), $\varepsilon_0 = 8.854 \times 10^{-12}\,Fm^{-1}$ is the vacuum permittivity, ε_r is 3.9 for SiO_2 and d is 300 nm for the thickness of SiO_2. The field-effect electron mobility of the 2D In_2Se_3 FETs was calculated to be $1\,cm^2\,V^{-1}\,s^{-1}$ in an ambient environment from the linear part of the transfer curve in figure 2(c), which is comparable to PVD-grown In_2Se_3 with a back-gated structure [25]. The current on/off ratio is another important parameter for evaluating the performance of a FET, which is determined by adopting a ratio of maximum to minimum I_{ds} from the transfer curves. The current on/off ratio was 10^3 for this 2D In_2Se_3 device as illustrated in the logarithmic transfer curve (figure 2(c)). Figure 2(d) shows the corresponding output curves measured when the gate voltage swept from −20 V to 20 V with 10 V/step. The output current decreased as the applied gate voltage swept from negative to positive values, which further confirms the n-type conductance property of the 2D In_2Se_3. The electronic performance of the 2D In_2Se_3 should be further improved by the elimination of wrinkles and organic residues introduced by the PMMA-assisted transfer process (as shown in figure S1).

In_2Se_3 with a narrow direct bandgap of 1.3 eV is a promising material for applications in optoelectronic devices, such as photodetectors. To investigate the photodetection performance of

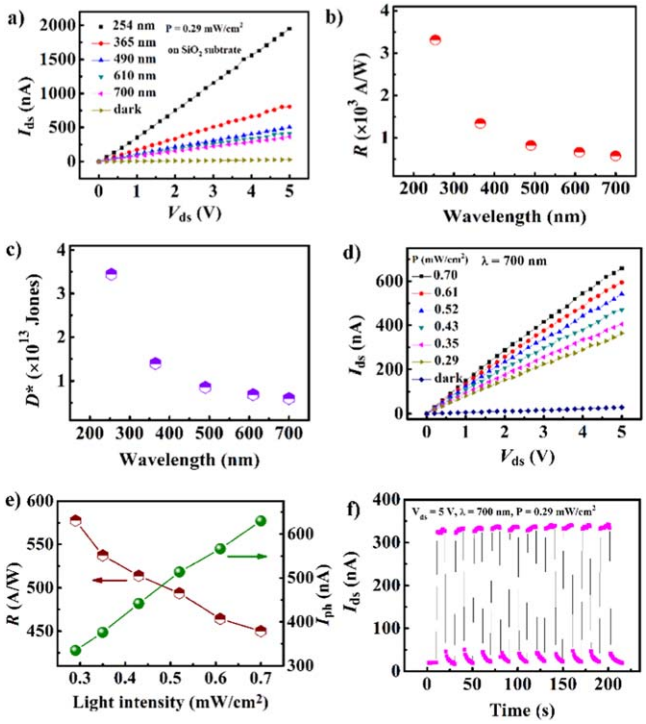

Figure 3. Photoresponse of 2D In_2Se_3 photodetector on rigid SiO_2/Si substrate. (a) The *I–V* curves of 2D In_2Se_3 photodetector under various illumination wavelengths (from 254 nm to 700 nm) with a light intensity of 0.29 mW · cm^{-2}. (b) The responsivity as a function of illumination wavelengths at $V_{ds} = 5$ V. (c) The detectivity as a function of illumination wavelengths at $V_{ds} = 5$ V. (d) The *I–V* curves of 2D In_2Se_3 photodetector on SiO_2/Si substrates under 700 nm light illumination with various light intensities. (e) The calculated I_{ph} and *R* as a function of light intensity under 700 nm at $V_{ds} = 5$ V. (f) The stability performance of rigid 2D In_2Se_3 photodetector under 700 nm switching on and off at $V_{ds} = 5$ V with a light intensity of 0.29 mW · cm^{-2}.

the 2D In_2Se_3 nanosheets, photodetectors were fabricated on a rigid SiO_2/Si substrate and a flexible PET substrate. First, we explored the photoresponse properties of the rigid 2D In_2Se_3 photodetectors. All the photoresponse measurements were conducted at $V_g = 0$ V in our study. Figure 3(a) shows the *I–V* curves of the rigid 2D In_2Se_3 photodetector measured under various illumination lights. The rigid 2D In_2Se_3 photodetector showed a broadband photoresponse range from ultraviolet (254 nm) to visible light (700 nm). To directly evaluate the photodetection performance of the 2D In_2Se_3 photodetector, three important parameters (photocurrent (I_{ph}), responsivity (*R*) and detectivity (D^*)) were extracted as a function of illumination light at $V_{ds} = 5$ V with a light intensity of 0.29 mW · cm^{-2}. From the equation $I_{ph} = I_i$-I_d, where I_i and I_d are the current measured with and without illumination, respectively, the values of I_{ph} can be calculated. As shown in figure S3, the I_{ph} was 335 nA for 700 nm light illumination and I_{ph} increased as the illumination light wavelength decreased. We could then calculate the *R* value using the following equation: $R = I_{ph}/P \cdot S$, where *P* is the light intensity and *S* is the channel area (200 μm^2). The calculated *R* value was 578 A W^{-1} for 700 nm light illumination and *R* increased as the wavelength decreased, as shown in figure 3(b), which is consistent with I_{ph}. The *R* value was 2 ∼ 8 times higher than those of the mechanically exfoliated few-layer In_2Se_3 nanosheets (395 A W^{-1} under 300 nm) [18] and PVD-grown 2D In_2Se_3 nanosheets (340 A W^{-1} under 532 nm) [25], which were also 2 ∼ 3 orders of magnitude higher than those of 2D GaSe (2.5 A W^{-1}) [13], currently commercial silicon and InGaAs photodetectors (<1 A W^{-1}) [28, 30]. The D^* value can be calculated by the equation: $D^* = RS^{1/2}/(2eI_d)^{1/2}$, where *R* is the responsivity, *S* is the area of the photodetector channel, *e* is the electron charge, and I_d is the dark current. The D^* value was 6.0×10^{12} Jones for 700 nm light as shown in figure 3(c). The D^* value was higher than those of mechanically exfoliated few-layer In_2Se_3 (2.26×10^{12} Jones) [18], currently commercial silicon and InGaAs photodetectors (10^{12} Jones) [30, 31]. Figure 3(d) shows *I–V* curves of the rigid 2D In_2Se_3 photodetector illuminated by 700 nm light under various light intensities. The I_{ph} linearly increased as the illumination light intensity increased, which demonstrates that generated I_{ph} was solely determined by the amount of photogenerated carriers under light illumination (shown in figure 3(e)). The calculated *R* values degraded with increasing light intensity, as shown in figure 3(e), which can be attributed to the trap states existing in the In_2Se_3 nanosheets or at the interface between the In_2Se_3 and SiO_2 substrate, which is similar to early reports of 2D In_2Se_3 photodetectors [27]. This behavior is well-known for trap-dominated photodetectors. As illumination light intensity increases, the longest-living trap states are filled and the shorter-living trap states begin to account for a significant component of the carrier lifetime. Therefore, the recombination probability of photogenerated electrons and holes will increase, which leads to a lower responsivity. To evaluate a photodetector, the stability and repeatability are also important parameters. As shown in figure 3(f), the 2D In_2Se_3 photodetector was illuminated under 700 nm with a bias voltage of 5 V and a light intensity of 0.29 mW · cm^{-2}. The 2D In_2Se_3 photodetector exhibited a stable and repeatable photoresponse after ten on/off cycles. To reveal the response time of the 2D In_2Se_3 photodetector, an enlarged time-resolved response with the light on and off is shown in figure S4. It can be clearly seen that the rise and fall times were 20 and 40 ms, respectively, which are comparable to that of a mechanically exfoliated 2D In_2Se_3 photodetector [18].

Next, we explore the photoresponse of the flexible 2D In_2Se_3 photodetector. The flexible and transparent photodetectors based on as-grown 2D In_2Se_3 nanosheets were fabricated on PET substrates (see section 2 for more detail). The inset in figure 4(a) is an optical image of a flexible 2D In_2Se_3 photodetector on a PET substrate. Figure 4(a) shows the *I–V* curves of a flexible 2D In_2Se_3 photodetector illuminated at various wavelength incident lights with a light intensity of 0.29 mW · cm^{-2}. It is obvious that the flexible 2D In_2Se_3 photodetector exhibited a wide photoresponse range from the ultraviolet (254 nm) to visible light (700 nm), which is similar to the results of the 2D In_2Se_3 photodetector on the rigid SiO_2 substrate. As shown in figure S5, the I_{ph} was 211 nA for 700 nm light and I_{ph} increased as the wavelength decreased, which is similar to results of the rigid photodetector. Noticeably, the generated I_{ph} of the flexible 2D In_2Se_3 photodetector on the PET substrate was lower than that of the rigid In_2Se_3 photodetector on the SiO_2 substrate. The

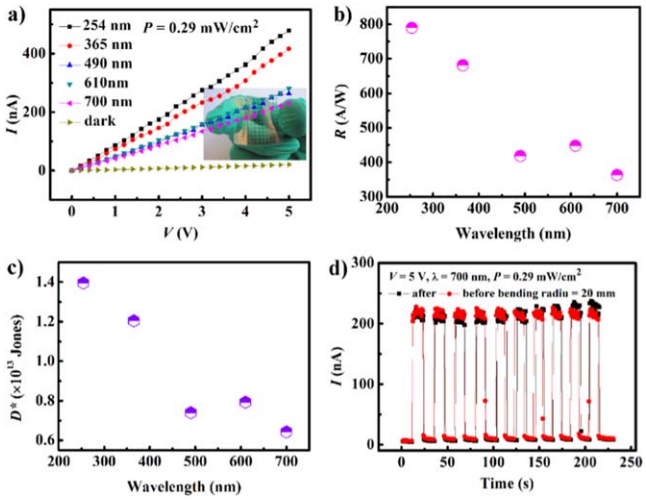

Figure 4. Photoresponse of flexible 2D In_2Se_3 photodetector. (a) The *I*–*V* curves of 2D In_2Se_3 photodetector on flexible PET substrates under various illumination wavelengths with a light intensity of 0.29 mW · cm^{-2}. Inset: optical image of flexible 2D In_2Se_3 photodetector. (b) Calculated *R* as a function of illumination wavelengths at $V_{ds} = 5$ V. (c) D^* as a function of illumination wavelengths at $V_{ds} = 5$ V. (d) The stability performance of flexible 2D In_2Se_3 photodetector before and after bending to 20 mm bending radius for 10 cycles switching on and off under 700 nm at $V_{ds} = 5$ V with a light intensity of 0.29 mW · cm^{-2}.

photon absorption was determined by multiple reflection interference at the interfaces of the semiconductor and substrates [32]. Because Si is non-transparent, In_2Se_3 nanosheets can absorb more photons by light multiple reflection, while PET is transparent and more photons go directly through the substrate rather than reflecting back. So it is reasonable that a flexible In_2Se_3 photodetector on a transparent PET substrate would generate a lower I_{ph}. The calculated *R* value was 363 A W^{-1} for 700 nm, as shown in figure 4(b), which is comparable to the value of the mechanically exfoliated few-layer In_2Se_3 nanosheets on the SiO_2 substrate (395 A W^{-1} under 300 nm at $V_{ds} = 5$ V) [18]. The D^* value of the flexible 2D In_2Se_3 photodetector was 6.4×10^{12} Jones for 700 nm light, shown in figure 4(c). The D^* value was higher than those of the mechanically exfoliated few-layer In_2Se_3 (2.26×10^{12} Jones) [18]. The mechanical stability and durability are important for a flexible photodetector. The mechanical stability and durability of the flexible 2D In_2Se_3 photodetectors were investigated by repeated bending. Figure 4(d) shows the photoresponse of the flexible In_2Se_3 photodetectors measured under on/off 700 nm light illumination before and after 10 repeated bending cycles with a bending radium of 20 mm. The flexible 2D In_2Se_3 photodetectors exhibited little variation in both the photocurrent and dark current after 10 repeated bending cycles, suggesting its excellent flexibility and mechanical durability. As shown in figure S6, the flexible 2D In_2Se_3 photodetectors showed a slower photoresponse speed with a rise time of 80 ms and a fall time of 70 ms compared to the rigid 2D In_2Se_3 photodetector. The photoresponse speeds of the flexible 2D In_2Se_3 photodetectors remained unchanged after bending, as seen in figure S6, further demonstrating its excellent flexibility.

4. Conclusion

In conclusion, the electronic and optoelectronic properties of CVD-grown 2D In_2Se_3 nanosheets were investigated for the first time. FETs based on CVD-grown 2D In_2Se_3 showed a typical n-type semiconducting behavior. 2D In_2Se_3 photodetectors were fabricated on rigid SiO_2/Si substrates and flexible PET substrates, and showed high photoresponse and a broadband photoresponse ranging from ultraviolet (254 nm) to visible light (700 nm). High photoresponsivities of 578 and 363 A · W^{-1} were achieved by rigid and flexible CVD-grown 2D In_2Se_3 photodetectors under 700 nm light illumination, respectively, which were higher than those of the mechanically exfoliated 2D In_2Se_3 and PVD-grown 2D In_2Se_3. Moreover, the flexible 2D In_2Se_3 photodetectors showed good mechanical durability and photoresponse stability under repeated bending testing. The high and stable photoresponse paves the way for CVD-grown 2D In_2Se_3 nanosheet applications in photodetector and photovoltaic devices.

Acknowledgments

This work is supported by the National Natural Science Foundation of China (NSFC, Nos. 51802038, 61390502 and 21373068), the China Postdoctoral Science Foundation (No. 2018M630329), the Fundamental Research Funds for the Central Universities (No. 2572018BC14), the Foundation for Innovative Research Groups of the National Natural Science Foundation of China (Grant No. 51521003), and the Self-Planned Task (Grant No. SKLRS201607B) of State Key Laboratory of Robotics and System (HIT).

ORCID iDs

Wei Feng https://orcid.org/0000-0001-6902-0024
PingAn Hu https://orcid.org/0000-0003-3499-2733

References

[1] Novoselov K S, Geim A K, Morozov S V, Jiang D, Zhang Y, Dubonos S V, Grigorieva I V and Firsov A A 2004 Electric field effect in atomically thin carbon films *Science* **306** 666
[2] Geim A K and Novoselov K S 2007 The rise of graphene *Nat. Mater.* **6** 183
[3] Novoselov K S, Jiang D, Schedin F, Booth T J, Khotkevich V V, Morozov S V and Geim A K 2005 Two-dimensional atomic crystals *Proc. Natl Acad. Sci.* **102** 10451
[4] Radisavljevic B, Radenovic A, Brivio J, Giacometti V and Kis A 2011 Single-layer MoS_2 transistors *Nat. Nanotechnol.* **6** 147
[5] Duesberg G S 2014 Heterojunctions in 2D semiconductors: a perfect match *Nat. Mater.* **13** 1075
[6] Kun H, Yucong Y, Ke L, Afzal K, Hui Z, Xiaodong P, Xuegong Y and Deren Y 2018 High and fast response of a graphene–silicon photodetector coupled with 2D fractal platinum nanoparticles *Adv. Opt. Mater.* **6** 1700793

[7] Ming H, Yucong Y, Kun H, Afzal K, Xiaodong Q, Dikai X, Hui Z, Xuegong Y and Deren Y 2018 Performance improvement of graphene/silicon photodetectors using high work function metal nanoparticles with plasma effect *Adv. Opt. Mater.* **6** 1701243

[8] Novoselov K S, Geim A K, Morozov S V, Jiang D, Katsnelson M I, Grigorieva I V, Dubonos S V and Firsov A A 2005 Two-dimensional gas of massless Dirac fermions in graphene *Nature* **438** 197

[9] Shi Y M *et al* 2010 Synthesis of few-layer hexagonal boron nitride thin film by chemical vapor deposition *Nano Lett.* **10** 4134

[10] Song L *et al* 2010 Large scale growth and characterization of atomic hexagonal boron nitride layers *Nano Lett.* **10** 3209

[11] Yin Z Y, Li H, Li H, Jiang L, Shi Y M, Sun Y H, Lu G, Zhang Q, Chen X D and Zhang H 2012 Single-layer MoS_2 phototransistors *ACS Nano* **6** 74

[12] Fang H, Chuang S, Chang T C, Takei K, Takahashi T and Javey A 2012 High-performance single layered WSe_2 p-FETs with chemically doped contacts *Nano Lett.* **12** 3788

[13] Baugher B W H, Churchill H O H, Yang Y F and Jarillo-Herrero P 2014 Optoelectronic devices based on electrically tunable p-n diodes in a monolayer dichalcogenide *Nat. Nanotechnol.* **9** 262

[14] Late D J, Liu B, Luo J J, Yan A M, Matte H, Grayson M, Rao C N R and Dravid V P 2012 GaS and GaSe ultrathin layer transistors *Adv. Mater.* **24** 3549

[15] Hu P A, Wen Z Z, Wang L F, Tan P H and Xiao K 2012 Synthesis of few-layer GaSe nanosheets for high performance photodetectors *ACS Nano* **6** 5988

[16] Mudd G W *et al* 2013 Tuning the bandgap of exfoliated InSe nanosheets by quantum confinement *Adv. Mater.* **25** 5714

[17] Feng W, Zheng W, Cao W W and Hu P A 2014 Back gated multilayer InSe transistors with enhanced carrier mobilities via the suppression of carrier scattering from a dielectric interface *Adv. Mater.* **26** 6587

[18] Jacobs-Gedrim R B, Shanmugam M, Jain N, Durcan C A, Murphy M T, Murray T M, Matyi R J, Moore R L and Yu B 2014 Extraordinary photoresponse in two-dimensional In_2Se_3 nanosheets *ACS Nano* **8** 514

[19] Lin M *et al* 2013 Controlled growth of atomically thin In_2Se_3 flakes by van der Waals epitaxy *J. Am. Chem. Soc.* **135** 13274

[20] Zhai T Y *et al* 2010 Fabrication of high-quality In_2Se_3 nanowire arrays toward high-performance visible-light photodetectors *ACS Nano* **4** 1596

[21] Lee H, Kang D H and Tran L 2005 Indium selenide (In_2Se_3) thin film for phase-change memory *Mater. Sci. Eng.* B **119** 196

[22] Yu B, Ju S Y, Sun X H, Ng G, Nguyen T D, Meyyappan M and Janes D B 2007 Indium selenide nanowire phase-change memory *Appl. Phys. Lett.* **91** 133119

[23] Julien C, Hatzikraniotis E, Chevy A and Kambas K 1985 Electrical behavior of lithium intercalated layered In–Se compounds *Mater. Res. Bull.* **20** 287

[24] Zheng W S *et al* 2015 Patterning two-dimensional chalcogenide crystals of Bi_2Se_3 and In_2Se_3 and efficient photodetectors *Nat. Commun.* **6** 6972

[25] Zhou J D, Zeng Q S, Lv D H, Sun L F, Niu L, Fu W, Liu F C, Shen Z X, Jin C H and Liu Z 2015 Controlled synthesis of high-quality monolayered a-In_2Se_3 via physical vapor deposition *Nano Lett.* **15** 6400

[26] Tao X and Gu Y 2013 Crystalline-crystalline phase transformation in two-dimensional In_2Se_3 thin layers *Nano Lett.* **13** 3501

[27] Island J O, Blanter S I, Buscema M, van der Zant H S J and Castellanos-Gomez A 2015 Gate controlled photocurrent generation mechanisms in high-gain In_2Se_3 phototransistors *Nano Lett.* **15** 7853

[28] Jorge Q, Robert B, Gabino R-B, Nicolás A, Roberto D A and Andres C-G 2016 Strong quantum confinement effect in the optical properties of ultrathin α-In_2Se_3 *Adv. Opt. Mater.* **4** 1939

[29] Feng W, Zheng W, Gao F, Chen X S, Liu G B, Hasan T, Cao W W and Hu P A 2016 Sensitive electronic-skin strain sensor array based on the patterned two-dimensional a-In_2Se_3 *Chem. Mater.* **28** 4278

[30] Yuang R-H, Chyi J-I, Lin W and Tu Y-K 1996 High-speed InGaAs metal–semiconductor–metal photodetectors with improved responsivity and process yield *Opt. Quant. Electron.* **28** 1327

[31] Monroy E, Omnès F and Calle F 2003 Wide-bandgap semiconductor ultraviolet photodetectors *Semicond. Sci. Technol.* **18** R33

[32] Feng W *et al* 2015 Ultrahigh photo-responsivity and detectivity in multilayer InSe nanosheets phototransistors with broadband response *J. Mater. Chem.* C **3** 7022